Geomechanics and Engineering, *Vol. 10, No. 2 (2016) 207-224*
DOI: http://dx.doi.org/10.12989/gae.2016.10.2.207

Effect of relative density on the shear behaviour of granulated coal ash

Norimasa Yoshimoto, Yang Wu*, Masayuki Hyodo and Yukio Nakata

Department of Civil Engineering, Yamaguchi University, Ube 755-8611, Japan

(*Received July 07, 2015, Revised November 23, 2015, Accepted December 11, 2015*)

Abstract. Granulated coal ash (GCA), a mixture of the by-product from milling processes with a small amount of cement added, has recently come to be used as a new form of geomaterial. The shear strength and deformation behaviours of GCA are greatly determined by its relative density or void ratio. A series of drained triaxial compression tests were performed on cylindrical specimens of GCA at confining pressures of between 50 kPa and 400 kPa at initial relative densities of 50%, 70% and 80%. Experimental results show that a rise in relative density increases the peak shear strength and intensifies the dilation behaviour. The initial tangent modulus and secant modulus of the stress-strain curve increase with increasing initial relative density, whereas the axial and volumetric strains at failure decrease with level of initial relative density. The stress-dilatancy relationships of GCA at different relative densities and confining pressures display similar tendency. The dilatancy behaviour of GCA is modelled by the Nova rule and the material property N in Nova rule of GCA is much larger than that of natural sand.

Keywords: granulated coal ash; relative density; drained shear property; friction angle; dilation

1. Introduction

Coal ash is an industrial byproduct of coal incineration in a coal fired thermal power plants. Due to the increasing demand for electricity, a vast amount of coal ash is produced yearly worldwide. The coal ash is recognized as waste and is a hazardous material to the surrounding environment due to its chemical composition. Because of this, it is necessary to find a good way in which to effectively use this deposited waste material. Usually, coal ash is disposed of with little consideration for engineering application, although it has been recognized that partial replacement of portland clinker with coal ash in cement can effectively improve the properties of the cement. Engineering methods reported by Kumar (2003), Pappu *et al*. (2007), Villamizar *et al*. (2012), Consoli *et al*. (2014) and Panich and Pitthaya (2014) of using coal ash and wastes to produce the building materials such as bricks have also been developed.

In the last three decades, the utilization of coal ash mixed with soil as a new form of geomaterial has attracted the attentions of many researchers (Horiuchi *et al*. 1992, 1995, Kawasaki *et al*. 1992, Consoli *et al*. 2007, Kim *et al*. 2011). The coal ash has been found to have some advantageous properties, such as light self-weight, higher consolidation rate, high shear strength and low cost. It has been demonstrated that the mechanical, physical and chemical properties of

*Corresponding author, Ph.D., E-mail: yangwuuu0226@hotmail.com

http://www.techno-press.org/?journal=gae&subpage=7 ISSN: 2005-307X (Print), 2092-6219 (Online)

coal ash vary for different coal types and morphology. Coal ash can be employed as a good alternative earth material instead of natural sand for ground construction, however, the wide and effective application of coal ash as a geomaterial requires a much better understanding of its mechanical and engineering properties.

The grain characteristics and engineering properties of coal ash have been investigated using coal ash with common mineralogical origins. Trivedi and Sud (2002) pointed out that some physical and mechanical indexes such as permeability and friction angle were strongly correlated with the mean grain size of the coal ash. Yoshimoto *et al*. (2005, 2007) studied the mechanical properties of granulated coal ash (GCA) which had similar grain size distribution to that of sand or fine gravel. Yoshimoto *et al*. (2012) and Wu *et al*. (2014) investigated the particle, compression and shear characteristics for different types of GCA. GCA tended to display large compressibility compared with natural sand and it was noted that the shear strength could be estimated based on the single particle strength, given that the confining pressure and density were known. Yoshimoto *et al*. (2014) presented that the both the cyclic shear strength and accumulative dissipated energy of GCA were larger than those of natural sands such as Toyoura sand due to the occurrence of particle crushing. The adoption of GCA in sand layer is beneficial for earthquake response and reducing the damage to the superstructure (Li *et al*. 2009, Shang *et al*. 2012, Yi *et al*. 2012).

It has been pointed out by researchers (Bolton 1986, Gutierrez 2003) that the shear strength of granular material is greatly determined by its relative density or void ratio, with the arrangement and interlocking of sand grains playing an influential role in the shear strength and deformation behaviours of granular assembly. Relative density D_r, a compaction specification index for granular material defined in Eq. (1), has been proven to be an influential factor affecting the stress-strain and volumetric behaviours of granular material in previous study (Park *et al*. 2008, Salot *et al*. 2009, Dash 2010, Mohamad *et al*. 2013, Zhuang *et al*. 2014, Wu and Yamamoto 2015).

$$D_r = (e_{\max} - e) / (e_{\max} - e_{\min}) \tag{1}$$

where $e_{\max}$ and $e_{\min}$ represent the maximum and minimum void ratios, and e is the void ratio at the current state. Although the dependence of the shear strength on the relative density of granular material has been discussed and confirmed by Tiwari and Shukla (2014), only a limited number of experimental studies on the influence of relative density on the shear strength and dilation behaviours of GCA have been conducted.

This study presents a systematic investigation on the effects of relative density and confining pressure on the shear strength and deformation behaviours of GCA. A series of drained triaxial compression tests were performed on GCA specimens at relative densities of 50%, 70% and 80%. The variations in the initial tangent modulus and secant modulus of the stress-strain curve, axial strain, volumetric strain, rate of dilation and friction angle at failure at variable relative densities and confining pressures are studied and compared. The stress-dilatancy relationship of GCA at different relative densities and confining pressures is also investigated and analyzed.

2. Physical properties of materials tested

Granulated coal ash is a mixture of the by-products from milling processes with a small amount of cement added. Some merits of using GCA as a geomaterial have been recognized, such as suppression of leaching of heavy metals and the possibility of outdoor curing. Another advantage

Table 1 Physical properties of granulated coal ash

	ρ_s (g/cm^3)	e_{max}	e_{min}	d_{50} (mm)	U_c	R_c	A_r
GCA	2.285	2.280	1.512	0.368	14.8	1.287	1.249

is that the particle strength and size of GCA can be changed manually, something which cannot be done with natural sand. The mixture is granulated using a mixing and rotating method. The round particle shape of GCA is manufactured in an industry-scale motor mixer with a capacity of 10.0 m^2. It is cured in the laboratory under natural dry conditions with a water content between 40% and 50%. Fig. 1 shows the appearance of GCA and an enlarged view of a single particle. The GCA is composed of coal ash, cement and kiln dust at a proportion of 85%, 5% and 10% by weight. Table 1 shows the physical properties of the GCA sample used in this test. The apparent density of GCA particles ρ_s is low compared to natural sand and it is believed that this is due to the presence of air vesicles in individual particles. The maximum void ratio e_{max} and minimum void ratio e_{min} of GCA are 2.280 and 1.512, which are also larger than those of natural sand. Manufactured GCA has a median diameter d_{50} of 0.368 mm and a coefficient of uniformity U_c of 14.8. The roundness coefficient R_c and aspect ratio A_r are also given in order to describe the particle shape of GCA.

Fig. 2 illustrates the grain size distribution curve of GCA. The particle size is intentionally adjusted to be similar to that of natural sand. The grain size distribution curve varies from

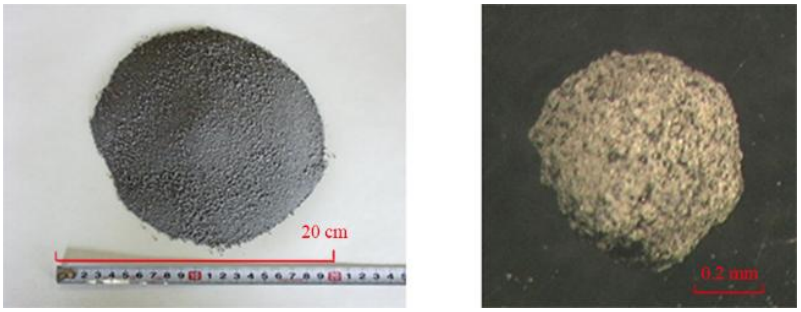

Fig. 1 Appearance and photography of granulated coal ash

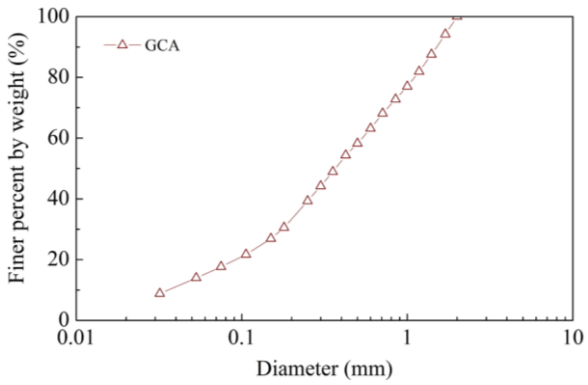

Fig. 2 Grain size distribution curve of GCA

0.03 mm to 2 mm. To be fit for the triaxial testing, particles with diameters equal to or larger than 2 mm were removed and the particle size grading curve was artificially adjusted to be well graded with a high coefficient of uniformity.

3. Testing apparatus and specimen

A low-pressure triaxial testing apparatus with the capacity of measuring the loading applied on and deformation of the specimen is used in this research. The apparatus has the capacity of providing a maximum axial load of 4.9 kN and a maximum confining pressure of 1 MPa. The pore pressure, axial loading and axial strain during shearing are synchronously recorded by a data-logger and computer.

Owing to the complex outer surfaces and existence of air voids inside the interior structure of GCA particles, it is very difficult to fully saturate specimens. In order to achieve the highest level of saturation possible, the specimen was first soaked in de-aired water and kept in a vacuum tank for three to four days in order to completely remove any air bubbles. Samples were saturated to a B value larger than 0.96. The specimens were water-pluviated into a mold with gently tapping until the target relative densities 50%, 70% and 80% were achieved. Although the efforts have been made to achieve the target initial relative density, there is still some scatter exists.

The cylindrical GCA specimen was 5 cm in diameter and 10 cm in height. The isotropic consolidation pressures applied on the specimens were 50 kPa, 100 kPa, 200 kPa, 300 kPa and 400 kPa. The consolidation pressure was increased gradually by 50 kPa increments. Table 2 gives the

Table 2 Experimental conditions about drained triaxial test on GCA at different confining pressures and relative densities

Relative density (%)	Confining pressure σ_c (kPa)	D_{ri} (%)	D_{rc} (%)	e_i	e_c	ρ_{di} (g/cm^3)	ρ_{dc} (g/cm^3)
D_r = 50	50	52.40	58.04	1.878	1.834	0.7941	0.8062
	100	52.54	64.22	1.876	1.787	0.7944	0.8199
	200	52.74	75.03	1.875	1.704	0.7948	0.8451
	300	52.64	82.74	1.876	1.645	0.7946	0.8640
	400	52.61	91.79	1.876	1.575	0.7945	0.8874
D_r = 70	50	67.93	69.37	1.758	1.747	0.8284	0.8317
	100	68.71	70.08	1.752	1.742	0.8302	0.8334
	200	68.85	78.08	1.751	1.680	0.8305	0.8525
	300	68.75	90.53	1.752	1.585	0.8303	0.8840
	400	69.08	93.43	1.749	1.562	0.8311	0.8917
D_r = 80	50	75.81	78.98	1.698	1.673	0.8470	0.8547
	100	74.47	81.31	1.708	1.656	0.8438	0.8605
	200	74.78	89.34	1.706	1.594	0.8445	0.8809
	300	74.73	93.95	1.706	1.558	0.8444	0.8931
	400	77.42	103.41	1.685	1.486	0.8509	0.9192

relative density D_r, void ratio e and dry density ρ_d of specimens before and after consolidation for GCA at different confining pressures and relative densities. The subscript i and c represent the states before and after consolidation. The triaxial shearing tests were performed at a constant speed rate of 0.1 mm/min until the critical state was reached.

4. Experimental results

Figs. 3-5 show the relationships between principal stress ratio, axial strain and volumetric strain of drained triaxial compression tests on GCA samples at relative densities of 50%, 70% and 80%, respectively. A dimensionless normalized stress index σ_a/σ_c is employed in the stress-strain relationship in order to investigate the mechanical characteristics of GCA under a wide range of confining pressures from 50 kPa to 400 kPa. σ_a is the axial stress on specimen and σ_c is the confining pressure.

The plot of principal stress ratio against axial strain for GCA at a relative density of 50% is displayed in Fig. 3(a). It can be observed that the steepness of the initial slope of the stress–strain curves reduces with increasing confining pressure. This change in the initial slope of the stress-

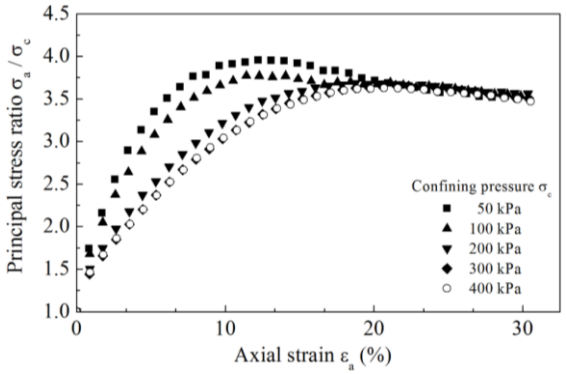

(a) Plot of principal stress ratio versus axial strain

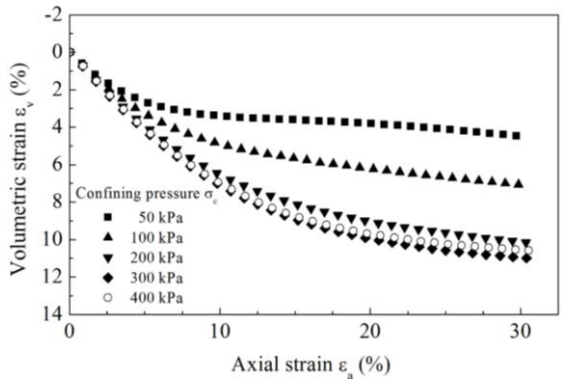

(b) Plot of volumetric strain versus axial strain

Fig. 3 Results of drained triaxial compression test on GCA at relative density D_r as 50% (Yoshimoto *et al.* 2012)

strain curve is due to the continual breakdown and rearrangement of the load bearing particles in the specimen during the increasing shearing stress. It can also be seen that the stress-strain curve shows a marked peak principal stress ratio at low confining pressures of 50 kPa and 100 kPa. The axial strain at which the peak principal stress ratio appears is around 10%. Experimental results demonstrate that the increasing confining pressure causes the failure of GCA at a larger axial strain. The stress-strain curve loses its sharpness as dilation behaviour is suppressed. Experimental results show that all stress-strain curves maintain a similar residual stress ratio once the axial strain exceeds 20%. Fig. 3(b) shows the volumetric strain plotted against axial strain of GCA at a relative density of 50%. Conventionally, the compression side is ruled to be positive in soil mechanics. Volumetric contraction becomes increasingly significant as the applied confining pressure is increased. The majority of volumetric change of GCA in loose state originates from the particle movement and rearrangement with some influence from particle crushing. No distinctive dilation of GCA specimen at relative density of 50% is observed due to the low single particle strength of GCA. The rate of the increasing volumetric strain gradually decreases and attains a steady value as the shearing stress continues.

The principal stress ratio plotted against the axial strain of specimens at relative densities of 70% and 80% are shown in Figs. 4(a) and 5(a). The peak principal stress ratio slightly increases as

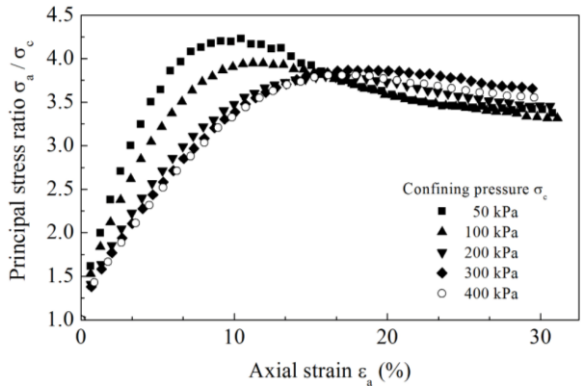

(a) Plot of principal stress ratio versus axial strain

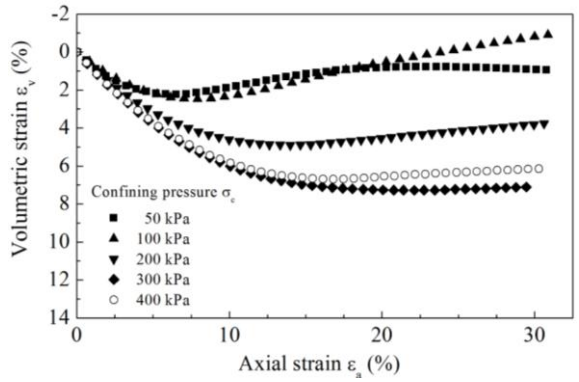

(b) Plot of volumetric strain versus axial strain

Fig. 4 Results of drained triaxial compression test on GCA at relative density D_r as 70%

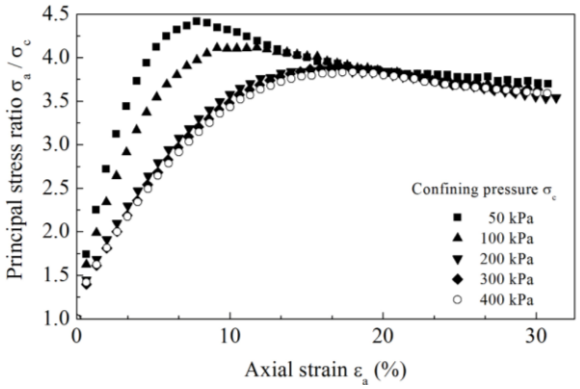

(a) Plot of principal stress ratio versus axial strain

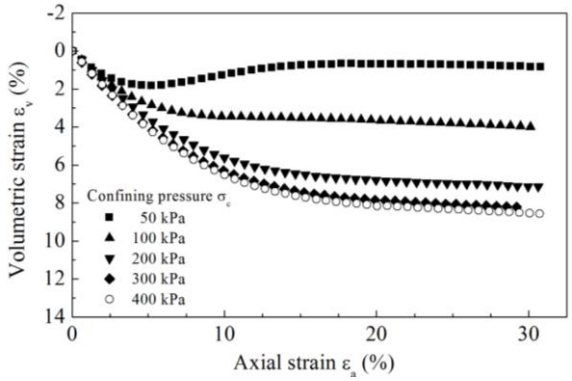

(b) Plot of volumetric strain versus axial strain

Fig. 5 Results of drained triaxial compression test on GCA at relative density D_r as 80%

the relative density increases. The rise in relative density also produces smaller strains at failure of the specimen at the same level of confining pressure. It is noted that the effect of relative density on the residual stress ratio appears to be minimal. Figs. 4(b) and 5(b) illustrate the volumetric strain plotted against the axial strain of GCA at relative densities of 70% and 80%. Dilative behaviour becomes noticeable as relative density is raised to 70% in Fig. 4(b). However, this increasing tendency of dilation behaviour of GCA at a relative density of 80% is not apparent in Fig. 5(b) due to the combined volumetric change originated from dilation and particle crushing. It should also be noted that the peak friction angle of clinker ash, which possessed similar mechanical features to GCA, markedly decreased with increasing confining pressure and it was explained that this was due to the occurrence of particle crushing by Winter *et al*. (2013). This variation in shear strength with the level of confining pressure is similar to other granular material discussed in Wu *et al*. (2013).

There exists a maximum rate of volumetric contraction at a confining pressure range between 300 kPa and 400 kPa in Fig. 3(b). The specimen has already been intensively compressed and as such increasing shearing stress causes less additional volumetric change. It is expected that some particles with larger diameter is slightly damaged under shearing stress and continually give rises to the dilation behaviour at confining pressure of 400 kPa in Fig. 4(b).

It is noted that principal stress ratios reach their peak values when the rate of volumetric change takes the maximum dilation value or the maximum volumetric contraction value. As such it can be understood that the rate of dilation plays a key role on the shear strength of GCA. The experimental results obtained are quite similar to those measured data in previous studies on other granular materials (Been and Jefferies 1985, Lade *et al*. 1996), indicating that GCA also exhibits similar mechanical features to other natural sands.

To examine the effect of the initial relative density on the shear strength and deformation behaviours, a comparison of the principal stress ratio-axial strain and volumetric strain-axial strain relationships of GCA at three relative densities and different confining pressures are exemplified as shown in Figs.6-7. The effect of relative density on the peak principal stress ratio and the initial slope of the stress-strain curve at low confining pressure is pronounced. Both the peak stress ratio and the initial slope of stress-strain curve increase with the level of relative density. Fig. 7 shows that volumetric contraction becomes increasingly predominant as the relative density reduces. In a loose state, the increased volumetric contraction continually reduces the rate of dilation at which the material can bear additional stress. GCA exhibits remarkable compressive characteristics compared to some other natural sands due to the observations of excessively volumetric contraction at a relatively low confining pressure of 400 kPa.

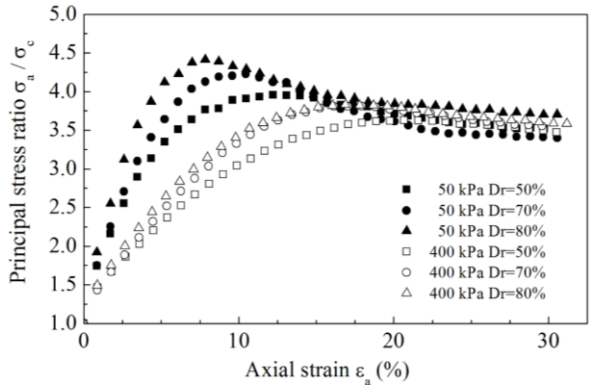

Fig. 6 Principal stress ratio plotted against axial strain for GCA at three levels of relative densities

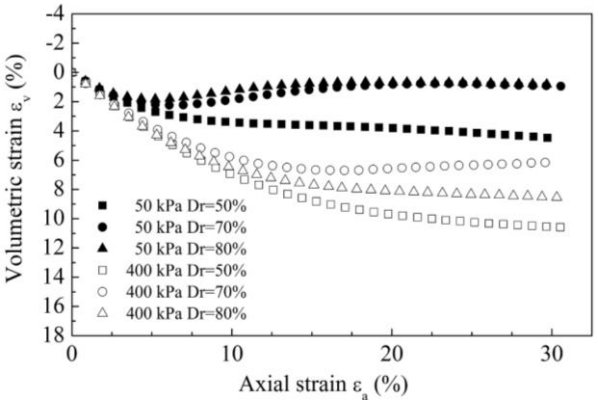

Fig. 7 Volumetric strain plotted against axial strain for GCA at three levels of relative densities

5. Effect of relative density on mechanical behaviour of GCA

5.1 Initial tangent modulus

The initial tangent modulus E_i in Eq. (2) is an influential parameter to describe the deformation behaviour of GCA at the starting stage of shearing. The initial tangent modulus E_i is determined by drawing the initial slope of the q- ε_a curve. Deviatoric stress q in Eq. (3) is the difference between the axial stress σ_a and the radial stress σ_r applied on the specimen. The radial stress σ_r is equivalent to the confining pressure σ_c in this study. The q- ε_a curve of GCA at different confining pressures and different relative densities are not shown here, but can be directly calculated from Figs. 3-5. To confirm that the deformation of GCA stays within the elastic range, measured results for determining the initial tangent modulus E_i are at an axial strain ε_a within 0.1%.

$$E_i = \frac{\Delta q}{\Delta \varepsilon_a} \tag{2}$$

where Δ means incremental value

$$q = \sigma_a - \sigma_c \tag{3}$$

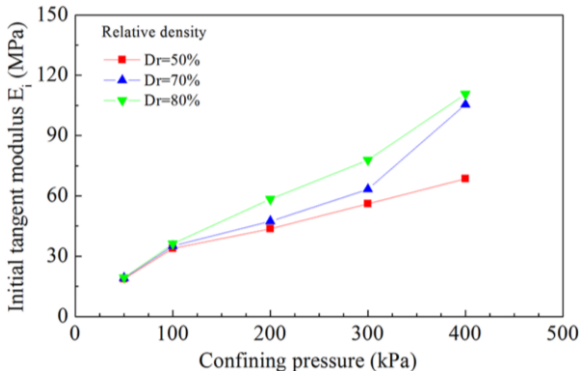

(a) At different relative densities

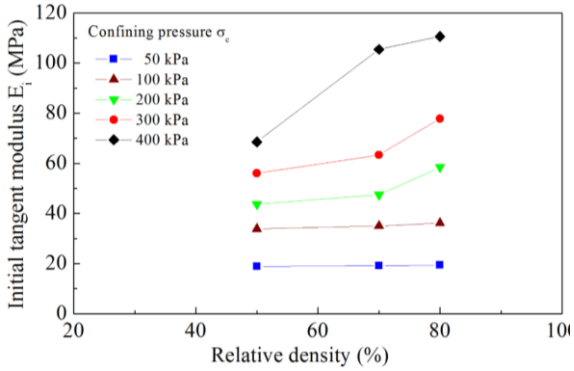

(b) At different confining pressures

Fig. 8 Variations in the initial tangent modulus

As can be seen in Fig. 8(a), the increasing rate of initial tangent modulus E_i with the level of confining pressure becomes obvious as the relative density increases. An increase in relative density of GCA specimens produces a larger initial tangent modulus E_i at confining pressures in the range from 200 kPa to 400 kPa. Fig. 8(b) shows that the initial tangent modulus E_i increases with a rise in confining pressure. Experimental results show that the initial tangent modulus E_i at different relative densities take almost the same value at a confining pressure of 50 kPa. The effect of relative density on the initial tangent modulus E_i of GCA at low confining pressure is minimal. However, this effect becomes increasingly pronounced as the confining pressure is increased.

5.2 Secant modulus at half of the peak strength

Fig. 9 displays the variation in the secant modulus at half of the peak strength value E_{50} of GCA at different confining pressures and relative densities. The secant modulus E_{50} has been regarded as an important model parameter in describing the stress-strain curve proposed by Duncan and Chang (1970) and is defined as the gradient of the secant line connecting the origin of coordinate and the point at half of the peak deviatoric stress q_{50} on the q-ε_a curve in Eq. (4). The peak deviatoric stress refers to the value of the peak point on the q-ε_a curve for strain softening behaviour or the

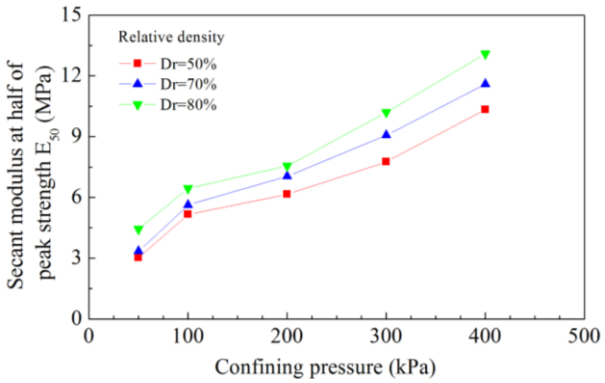

(a) At different relative densities

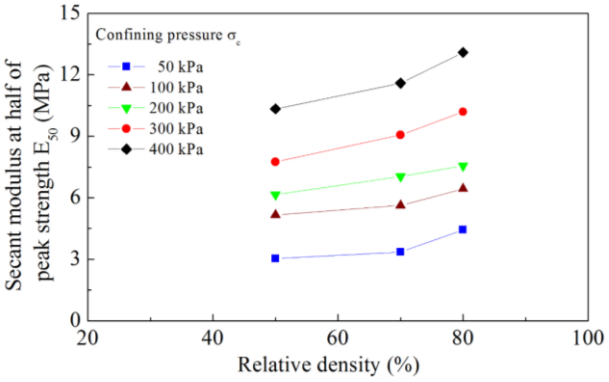

(b) At different confining pressures

Fig. 9 Variations in the secant modulus at half of the peak strength

Table 3 Initial tangent modulus and secant modulus at half of peak strength of GCA at different confining pressures and relative densities

Confining pressure σ_c (kPa)	Initial tangent modulus E_i (MPa)			Secant modulus at half of peak strength E_{50} (MPa)		
	D_r = 50%	D_r = 70%	D_r = 80%	D_r = 50%	D_r = 70%	D_r = 80%
50	18.846.	19.151	19.384	3.033	3.349	4.436
100	33.817	35.027	36.175	5.160	5.625	6.444
200	43.675	47.405	58.398	6.154	7.042	7.556
300	56.031	63.325	77.794	7.753	9.069	10.199
400	68.528	105.471	110.619	10.336	11.591	13.087

stress at critical state for strain hardening behaviour. It is indicated that the residual stress attains a constant value and is less dependent on confining pressure. The critical state stress ratio is assumed to be equal to the residual stress ratio when the specimen enters into the critical state. It is noted that the secant modulus at half of the peak strength E_{50} increases with the increasing relative density in Fig. 9(a). Initially, the secant modulus E_{50} increases rapidly at low confining pressure, with this increase becoming more gradual when the confining pressure exceeds100 kPa.

$$E_{50} = \frac{q_{50}}{\varepsilon_a} \tag{4}$$

Fig. 9(b) shows that the secant modulus E_{50} of GCA increases as the relative density is increased. However, this increasing tendency is less dependent on the confining pressure level.

It can be ascertained that both of the initial tangent modulus E_i and secant modulus E_{50} of GCA are greatly influenced by the levels of relative density and confining pressure. Table 3 shows the initial tangent modulus E_i and secant modulus E_{50} of GCA at different confining pressures and relative densities.

5.3 Axial strain at failure

Fig. 10 illustrates that the axial strain at failure (from the principal stress ratio - axial strain curve) plotted against the mean normal stress p at failure in Eq. (5) for a series of drained triaxial compression tests on GCA specimens at three relative densities. The experiment produces relatively small axial strains of less than 12% at low mean normal stress and relative density of 50%. A rapid increase in axial strain at failure resulted from the complete densification and particle crushing in the specimen during shearing at mean normal stresses between 200 kPa to 400 kPa, as shown in Fig. 10. The axial strain at failure slowly increases and gradually attains a steady value as the mean normal stress continues. The observed reduction of axial strain at failure at high mean normal stress illustrated by Lade and Bopp (2005), Bopp and Lade (2005) for natural sand cannot be captured in this study. This is due to that the mean normal stress applied on the GCA specimen is not high enough to cause a large amount of particles to be sufficiently crushed.

$$p = \frac{(\sigma_a + 2\sigma_c)}{3} \tag{5}$$

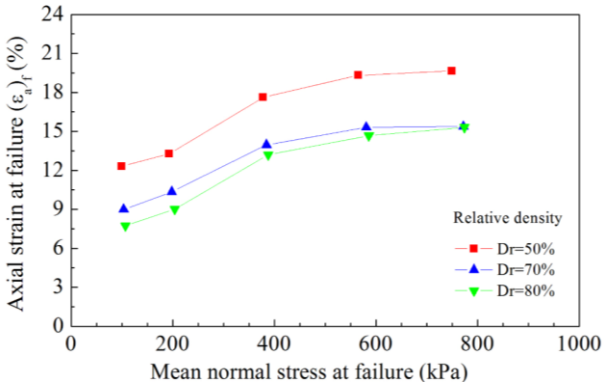

Fig. 10 Comparison of the axial strain at failure for drained triaxial compression on GCA at three levels of relative densities

Fig. 10 shows that an increase in relative density causes specimens to fail at lower axial strains. The particles in densely packed specimen are surrounded by a large number of neighboring particles and can sustain an additional shear stress at a relatively earlier stage. The interlocking mechanism in dense specimen is fully exerted at a smaller axial strain level. The movement and rearrangement of the particles in loose specimen during initial shearing delays the appearance of axial strain at failure.

5.4 Volumetric strain at failure

Fig. 11 shows the volumetric strain at failure plotted against the mean normal stress at failure of GCA at three relative densities. Volumetric strain at failure increases with increasing mean normal stress to a maximum value, after which it begins to decrease with increasing mean normal stress. This is due to the volumetric contraction caused by consolidation and the volumetric change induced by shearing at high confining pressures. The combined compressive and shearing volumetric variations almost reach a limit and the rate of dilation in the corresponding pressure region is reduced to a quite small value at high mean normal stress.

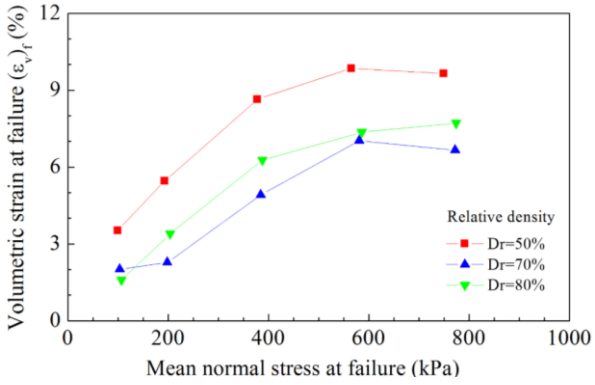

Fig. 11 Comparison of the volumetric strain at failure for drained triaxial compression on GCA at three levels of relative densities

Being similar to the axial strain at failure, experimental results of the volumetric strain at failure of GCA exhibit a decreasing tendency as the relative density is increased from 50% to 70% and 80%. However, the experiments produce relatively larger volumetric strains but at a higher relative density of 80%. It is expected that additional volumetric contraction is caused by the additional volumetric contraction from particle crushing within the relatively dense specimen.

5.5 Rate of dilation at failure

Fig. 12 shows the plot of the rate of dilation at failure $(d\varepsilon_v^p/d\varepsilon_s^p)_f$ against the mean normal stress at failure for GCA at three relative densities. $d\varepsilon_v^p$ and $d\varepsilon_s^p$ are the plastic volumetric strain and plastic shear strain rates, respectively. The plastic part of volumetric and shear strain rates are obtained by extracting the elastic portions from the total strains using a central-difference method in Eqs. (6) and (7). Negative values for the rate of dilation indicates that volume tends to dilate during shearing. In contrast, positive values for the rate of dilation means that the volume exhibits contractive behaviour under shearing.

$$d\varepsilon_v^p=(\varepsilon_{v,j+1}-\varepsilon_{v,j-1})-(p_{j+1}-p_{j-1})/K \tag{6}$$

$$d\varepsilon_s^p=(\varepsilon_{s,j+1}-\varepsilon_{s,j-1})-(q_{j+1}-q_{j-1})/3G \tag{7}$$

where the subscript j indicates the step number recorded by computer in testing. K and G are the elastic bulk and shear modulus and assumed to be constant between the two strains at step $j+1$ and $j-1$. The method to calculate the rate of dilation was also adopted by Been and Jefferies (2004).

GCA exhibits the dilative behaviour in corresponding to the peak stress ratio at low stress magnitude at relative densities of 70% and 80%. With an increasing amount of volumetric contraction originated from particle crushing and rearrangement at higher stress magnitudes, the rate of dilation at failure at each relative density exhibits a decreasing tendency with increasing mean normal stress. It is noted that the rate of dilation at failure varies from negative values to positive values for GCA specimen at relative densities of 70% and 80% over a wide range of confining pressures from low to high. However, the initial value for rate of dilation at failure for

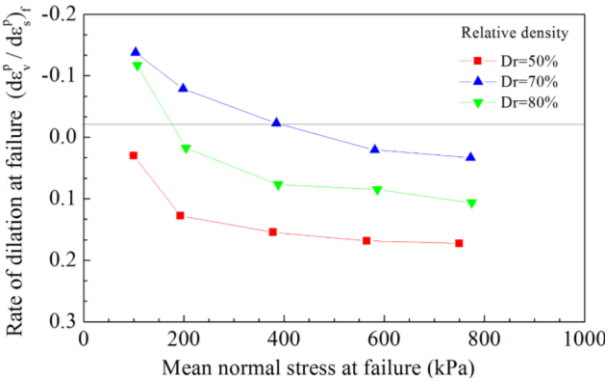

Fig. 12 Comparison of the rate of dilation at failure for drained triaxial compression on GCA at three levels of relative densities

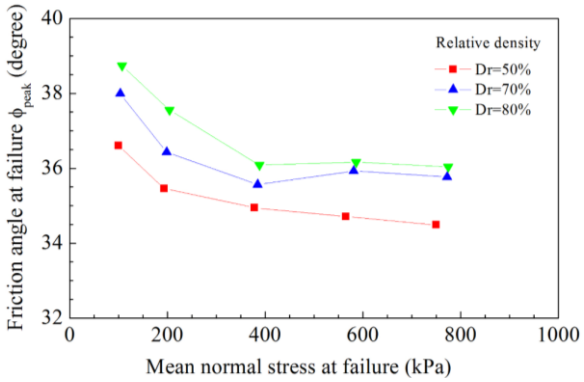

Fig. 13 Comparison of the friction angle at failure for drained triaxial compression on GCA at three levels of relative densities

GCA specimens in a loose state is positive. The slope of the curve rapidly decreases at low mean normal stress and this decreasing tendency becomes slower at high mean normal stress. Experimental results demonstrate that the increasing relative density from 50% to 70% or 80% results in a decreasing dilation rate during the entire loading process.

5.6 Friction angle at failure

The variation in the friction angle at failure at three relative densities over a wide range of confining pressures are shown in Fig. 13. The friction angle at failure of GCA increases with the level of relative density. The friction angle is an important parameter for evaluating the shear strength of granular material. Under triaxial compression condition, the friction angle at peak value ϕ_{peak} can be determined by the stress ratio at failure $(q/p)_{peak}$ in Eq. (8) and regarded as the friction angle at failure (Atkinson and Bransby 1977).

$$\left(\frac{q}{p}\right)_{peak} = \frac{6\sin\phi_{peak}}{3-\sin\phi_{peak}} \tag{8}$$

Experimental results show that the fiction angle at failure ϕ_{peak} initially decreases as the mean normal stress at failure increases. This phenomena is due to the progressive reduction in dilative behaviour with increasing mean normal stress as shown in Fig. 12. The friction angle decreases markedly for GCA at mean normal stress less than 400 kPa and maintains a stabilized value as mean normal stress is increased to higher magnitudes. Friction angles at failure are determined as 39.1℃, 38.0℃ and 36.8℃ for GCA at a confining pressure of 50 kPa at relative densities of 80%, 70% and 50%, respectively. It is estimated that the friction angle at failure loses almost three degrees as the applied mean normal stress on GCA attains the maximum value of 400 kPa at each level of relative density in this study.

6. Stress-dilatancy relationship

The feature of stress-dilatancy relationship is to capture the evolutions of strain increment and

stress ratio of granular material in drained triaxial compression test. Properly modelling the stress-dilatancy of granular material is an important criterion in the usefulness of any elasto-plastic constitutive model of granular material. The investigation on stress-dilatancy relationship for granular material had been intensively conducted (Taylor 1948, Roscoe *et al*. 1963, Roscoe and Burland 1968, Wan and Guo 1998).

Fig. 14 shows the stress ratio (q / p) plotted against the rate of dilation of GCA during the entire loading at three relative densities and at confining pressures of 50 kPa and 400 kPa. The stress-dilatancy relationship of GCA are quite similar at different relative densities. For GCA at three relative densities, the initial path of the stress-dilatancy shows liner relationship at low stress ratio. The path of stress-dilatancy reverses once the rate of dilation attains its peak value. The "hook" in the stress-dilatancy curve has also been observed for GCA as previous report on the other granular material by Been and Jefferies (2004). Experimental results represent that the inclination of stress-dilatancy curve at higher stress ratio becomes steeper as confining pressure is decreased. However, it is noted that the effect of relative density on the stress-dilatancy of GCA at high stress ratio becomes less remarkable.

The flow rule proposed by Nova (1982) in Eq. (9) is employed to evaluate and model the dilatancy behaviour of GCA.

$$D = (M - \eta) / (1 - N) \tag{9}$$

where $D = d\varepsilon_v/d\varepsilon_s$ is the dilatancy function and M is the stress ratio at critical state. $d\varepsilon_v$ and $d\varepsilon_s$ are the total volumetric strain rate and total shear strain rate. As the shearing stress continues, the elastic strain portion is far smaller than the corresponding plastic portion. Thus, the dilatancy function D is approximately treated as the same to the rate of dilation $d\varepsilon_v^p/d\varepsilon_s^p$ in section 5.5. N is a density-independent material property and reviewed as a volumetric coupling coefficient. Due to the compression-positive convention, the stress ratio at peak point η_{peak} corresponds to the minimum value of the dilatancy function D_{min}.

Fig. 15 presents the (η_{peak}-M)/ (1-N) plotted versus D_{min} data of GCA at different relative densities and the trend line computed using Nova stress-dilatancy equation. N can be determined from the slope of the approximation line for experimental results between (η_{peak}-M) and $D_{\min}$. N for GCA takes the value as 0.58 which is much higher than that of natural sand. It is revealed by Jefferies (1993) that N can be regarded as a crushability index of sand, with a larger N value

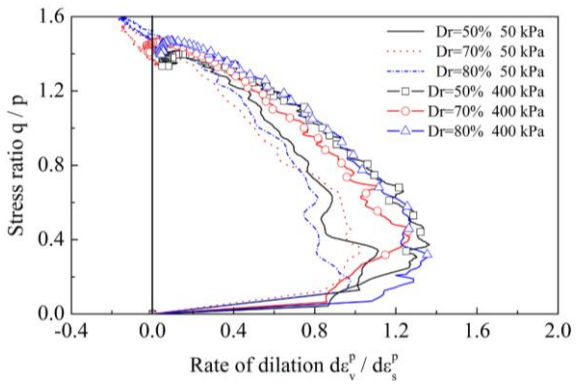

Fig. 14 Stress-dilatancy of GCA at different relative densities and confining pressures

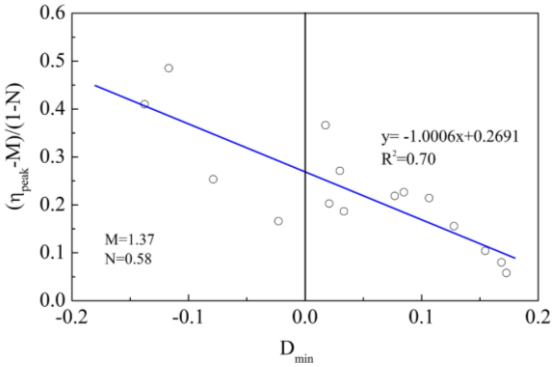

Fig. 15 Measured dilatancy of GCA at three levels of relative densities

representing a more crushable material. That is the reason why some results for $D_{\min}$ of GCA are positive even at low stress magnitude.

7. Conclusions

A series of drained triaxial compression tests on cylindrical specimens of GCA under a wide range of confining pressures from 50 kPa to 400 kPa were conducted in order to examine the effect of relative density and confining pressure on the shear strength and deformation behaviour. The major findings of this study are summarized below.

(1) Experimental investigations show consistent mechanical behaviour of GCA subjected to drained triaxial compression at from low to high confining pressures. It is noted that the peak principal stress ratio of GCA decreases with the increasing confining pressure and decreasing relative density. However, the residual stress ratio is less dependent on the level of confining pressure. The effect of particle crushing on the stress-strain curve of GCA is obvious.

(2) The initial tangent modulus of GCA increases with an increase in confining pressure. The effect of relative density on the initial tangent modulus of GCA at low confining pressure is minimal. The initial values of the initial tangent modulus of GCA at all three relative densities at low confining pressure are almost the same. The effect of relative density becomes increasingly pronounced as the confining pressure is increased.

(3) The secant modulus at half of the peak strength of GCA increases as the relative density increases. A rapid rise in secant modulus at half of the peak strength is observed at low confining pressure and this increasing tendency slows down as the confining pressure exceeds 100 kPa. The tendency for the secant modulus at half of the peak strength value to increase with increasing relative density is not affected by the level of confining pressure.

(4) The rise in relative density of GCA specimens leads to smaller axial and volumetric strains at failure. The axial strain at failure rapidly increases at low mean normal stress and gradually attains a steady value as the mean normal stress progresses. Volumetric strain at failure increases to a maximum value and slightly decreases as the confining pressure varies from low to high.

(5) The effect of relative density on the rate of dilation and friction angle at failure is apparent

at low confining pressure and becomes less remarkable as confining pressures increases. The decreasing tendencies of the rate of dilation and friction angle at failure with a rise in confining pressure are represented. Experimental results demonstrate that the rate of dilation at failure is closely correlated with the friction angle at failure of GCA in drained triaxial compression test.

(6) The stress-dilatancy relationship of GCA at different relative densities and confining pressures is similar. The inclination of stress-dilatancy curve at a higher stress ratio (q / p) becomes steeper as confining pressure is decreased. The dilatancy behaviour of GCA at different densities and confining pressures is modelled by the Nova rule. In comparison with natural sand, GCA owns a larger value of the material property N which is adopted as the crushability index in Nova rule. A larger N value indicates a more crushable material.

References

Atkinson, J.H. and Bransby, P.L. (1977), *The Mechanics of Soils, An Introduction to Critical State Soil Mechanics*, McGRAW-HILL, Maidenhead, Berkshire, England.

Been, K. and Jefferies, M.G. (1985), "A state parameter for sands", *Geotechnique*, **35**(2), 99-112.

Been, K. and Jefferies, M. (2004), "Stress-dilatancy in very loose sand", *Can. Geotech. J.*, **41**(5), 972-989.

Bolton, M.D. (1986), "The strength and dilatancy of sands", *Geotechnique*, **36**(1), 65-78.

Bopp, P.A. and Lade, P.V. (2005), "Relative density effects on undrained sand behavior at high pressures", *Soils Found.*, **45**(1), 15-26.

Consoli, N.C., Heineck, K.S., Coop, M.R., Fonseca, A.V.D. and Ferreira, C. (2007), "Coal bottom ash as a geomaterial: Influence of particle morphology on the behavior of granular materials", *Soils Found.*, **47**(2), 361-373.

Consoli, N.C., Rocha, C.G.D. and Saldanha, R.B. (2014), "Coal fly ash-carbide lime bricks: An environment friendly building product", *Construct. Build. Mater.*, **69**, 301-309.

Dash, S.K. (2010), "Influence of relative density of soil on performance of Geocell-reinforced Sand Foundation", *J. Mater. Civ. Eng.*, **22**(5), 533-538.

Duncan, J.M. and Chang, C.Y. (1970), "Nonlinear analysis of stress and strain in soils", *J. Soil. Mech. Found. Div.*, **96**(5), 1629–1653.

Gutierrez, M. (2003), "Modelling of the steady-state response of granular soils", *Soils Found.*, **43**(5), 95-105.

Horiuchi, S., Taketsuka, M., Odawara, T. and Kawasaki, H. (1992), "Fly-Ash Slurry Island: I. Theoretical and experimental investigations", *J. Mater. Civ. Eng.*, **4**(2), 117-133.

Horiuchi, S., Tamaoki, K. and Yasuhara, K. (1995), "Coal ash slurry for effective underwater disposal", *Soils Found.*, **35**(1), 1-10.

Jefferies, M.G. (1993), "Nor-Sand: A simple critical state model for sand", *Geotechnique*, **43**(1), 91-103.

Kawasaki, H., Horiuchi, S., Akatsuka, M. and Sano, S. (1992), "Fly-Ash Slurry Island: II. Construction in Hakucho Ohashi Project", *J. Mater. Civ. Eng.*, **4**(2), 134-152.

Kim, Y.T., Lee, C. and Park, H.I. (2011), "Experimental Study on Engineering Characteristic of Composite Geomaterial for Recycling Dredged Soil and Bottom Ash", *Mar. Georesour. Geotec.*, **29**(1), 1-15.

Kumar, S. (2003), "Fly ash-lime-phosphogypsum hollow blocks for walls and partitions", *Build. Environ.*, **38**(2), 291-295.

Lade, P.V. and Bopp, P.A. (2005), "Relative density effects on drained sand behavior at high pressures", *Soils Found.*, **45**(1), 1-13.

Lade, P.V., Yamamuro, J. and Bopp, P.A. (1996), "Significance of particle crushing in granular materials", *J. Geotech. Engrg.*, **122**(4), 309-316.

Li, H.N., Yi, T.H., Gu, M. and Huo, L.S. (2009), "Evaluation of earthquake-induced structural damages by wavelet transform", *Prog. Nat. Sci.*, **19**(4), 461-470.

Mohamad, E.T., Latifi, N., Marto, A., Moradi, R. and Abad, S. (2013), "Effects of relative density on shear

strength characteristics of sand-tie chips mixture", *Electronic. J. Geotech. Eng.*, **18**, 623-632.
Nova, R. (1982), "*A Constitutive Model for Soil under Monotonic and Cyclic Loading. Soil mechanics-transient and cyclic loads*", John Wiley & Sons, New York, USA.
Panich, V. and Pitthaya, J. (2014), "Characteristics of expansive soils improved with cement and fly ash in Northern Thailand", *Geomech. Eng., Int. J.*, **6**(5), 437-453.
Pappu, A., Saxena, M. and Asolekar, S.R. (2007), "Solid wastes generation in India and their recycling potential in building materials", *Build. Environ.*, **42**(6), 2311-2320.
Park, L.K., Suneel, M. and Chul, I.J. (2008), "Shear strength of Jumunjin sand according to relative density", *Mar. Georesour. Geotec.*, **26**(2), 101-110.
Roscoe, K.H. and Burland, J.B. (1968), "On the generalized stress-strain behaviour of wet clay", *Eng. Plast.*, 535-609.
Roscoe, K.H., Schofield, A.N. and Thurairajah, A. (1963), "Yielding of Clays in State Wetter than Critical", *Geotechnique*, **13**(3), 211-240.
Salot, C., Gotteland, P. and Villard, P. (2009), "Influence of relative density on granular materials behavior: DEM simulations of triaxial tests", *Granul. Matter.*, **11**(4), 221-236.
Shang, H.S., Yi, T.H. and Yang, L.S. (2012), "Experimental study on the compressive strength of big mobility concrete with nondestructive testing method", *Adv. Mater. Sci. Eng.*, ID 345214.
Taylor, D.W. (1948), *Fundamentals of Soil Mechanics*, John Wiley, New York, NY, USA.
Tiwari, A. and Shukla, S.K. (2014), *Advanced Carbon Materials and Technology*, John Wiley and Sons, Inc., Hoboken, NJ, USA.
Trivedi, A. and Sud, V.K. (2002), "Grain characteristics and engineering properties of coal ash", *Granul. Matter.*, **4**(3), 93-101.
Villamizar, M.C.N., Araque, V.S., Reyes, C.A.R. and Silva, R.S. (2012), "Effect of the addition of coal-ash and cassava peels on the engineering properties of compressed earth blocks", *Constr. Build. Mater.*, **36**, 276-286.
Wan, R.G. and Guo, P.J. (1998), "A simple constitutive model for granular soils: modified stress-dilatancy approach", *Comput. Geotech.*, **22**(2), 109-133.
Winter, M., Ohara, N., Hyodo, M., Nakata, Y., Yoshimoto, N., Yoshioka, I. and Nakashita, A. (2013), "Effect of particle strength on the monotonic shear strength of clinker ash", *Geo. Lett.*, **3**(3), 112-118.
Wu, Y. and Yamamoto, H. (2015), "Numerical Investigation on the Reference Crushing Stress of Granular Materials in Triaxial Compression Test", *Period. Polytech. Civil Eng.*, **59**(4), 465-474.
Wu, Y., Yamamoto, H., Yao, Y.P. (2013), "Numerical study on bearing behavior of pile considering sand particle crushing", *Geomech. Eng., Int. J.*, **5**(3), 241-261.
Wu, Y., Yoshimoto, N., Hyodo, M. and Nakata, Y. (2014), "Evaluation of crushing stress at critical state of granulated coal ash in triaxial test", *Geo. Lett.*, **4**(4), 337-342.
Yi, T.H., Li, H.N. and Zhao, X.Y. (2012), "Noise smoothing for structural vibration test signals using an improved wavelet thresholding technique", *Sensors*, **12**(8), 11205-11220.
Yoshimoto, N., Hyodo, M., Nakata, Y., Murata, H., Hongo, T. and Ohnaka, A. (2005), "Particle characteristics of granulated coal ash as geomaterial", *J. Soc. Mater. Sci.*, **54**(11), 1111-1116. [In Japanese]
Yoshimoto, N., Hyodo, M., Nakata, Y. and Orense, R.P. (2007), "An examination of the utilization of granulated coal as geomaterial based on particle strength", *Tsuchi to Kiso*, **55**(10), 23-25. [In Japanese]
Yoshimoto, N., Hyodo, M., Nakata, Y., Orense, R.P., Hongo, T. and Ohnaka, A. (2012), "Evaluation of shear strength and mechanical properties of granulated coal ash based on single particle strength", *Soils Found.*, **52**(2), 321-334.
Yoshimoto, N., Orense, R.P., Hyodo, M. and Nakata, Y. (2014), "Dynamic behavior of Granulated coal ash during earthquake", *J. Geotech. Geoenviron.*, **140**(2), 04013002.
Zhuang, L., Nakata, Y., Kim, U.G. and Kim, D. (2014), "Influence of relative density, particle shape, and stress path on the plane strain compression behavior of granular materials", *Acta. Geotech.*, **9**(2), 241-255.

CC